Synapse-Specific Contribution of the Variation of Transmitter Concentration to the Decay of Inhibitory Postsynaptic Currents

Zoltan Nusser,* David Naylor,† and Istvan Mody*

*Department of Neurology, UCLA School of Medicine, and †VA Greater Los Angeles Health Care System, Los Angeles, California 90095-1769 USA

ABSTRACT Synaptic transmission is characterized by a remarkable trial-to-trial variability in the postsynaptic response, influencing the way in which information is processed in neuronal networks. This variability may originate from the probabilistic nature of quantal transmitter release, from the stochastic behavior of the receptors, or from the fluctuation of the transmitter concentration in the cleft. We combined nonstationary noise analysis and modeling techniques to estimate the contribution of transmitter fluctuation to miniature inhibitory postsynaptic current (mIPSC) variability. A substantial variability (~30%) in mIPSC decay was found in all cell types studied (neocortical layer2/3 pyramidal cells, granule cells of the olfactory bulb, and interneurons of the cerebellar molecular layer). This large variability was not solely the consequence of the expression of multiple types of $GABA_A$ receptors, as a similar mIPSC decay variability was observed in cerebellar interneurons that express only a single type ($\alpha_1\beta_2\gamma_2$) of $GABA_A$ receptor. At large synapses on these cells, all variance in mIPSC decay could be accounted for by the stochastic behavior of ~36 pS channels, consistent with the conductance of $\alpha_1\beta_2\gamma_2$ $GABA_A$ receptors at physiological temperatures. In contrast, at small synapses, a significant amount of variability in the synaptic cleft GABA transient had to be present to account for the additional variance in IPSC decay over that produced by stochastic channel openings. Thus, our results suggest a synapse-specific contribution of the variation of the spatiotemporal profile of GABA to the decay of IPSCs.

INTRODUCTION

A fundamental feature of chemical synaptic transmission is the remarkable trial-to-trial variability of the postsynaptic responses (del Castillo and Katz, 1954; Redman, 1990; Stevens, 1993). It has been long recognized that the probabilistic nature of quantal neurotransmitter release (Allen and Stevens, 1994; del Castillo and Katz, 1954) accounts for a significant portion of this variability. If the transmitter release probability is low, synaptic connections become unreliable, profoundly affecting the way in which information is transmitted between neurons (Lisman, 1997; Zador, 1998). Increasing the number of synaptic release sites between two neurons improves reliability (Zador, 1998). Additional variability of postsynaptic responses, that is independent of the probabilistic nature of transmitter release, originates from the stochastic behavior of postsynaptic receptors (Faber et al., 1992) or from fluctuations in the peak concentration and time course of transmitter in the synaptic cleft. In the present study we estimated the contribution of transmitter fluctuation to the postsynaptic response variability. As currently there is no available method to directly monitor the spatiotemporal profile of neurotransmitter concentration in the synaptic cleft, there are only indirect ways to estimate the peak concentration and the rate of transmitter clearance (Bergles et al., 1999; Clements, 1996; Clements et al., 1992; Colquhoun et al., 1992; Jones and Westbrook, 1995; Maconochie et al., 1994; Mozrzymas et al., 1999; Perrais and Ropert, 1999). There is very little information available regarding the trial-to-trial variability of these parameters at individual central synapses. The relatively large variation in the peak amplitude of postsynaptic currents (PSCs) observed at single release sites is consistent with not all postsynaptic receptors being occupied by the released transmitter. Consequently, there should be a significant fluctuation in the peak transmitter concentration to account for the quantal amplitude variance (Auger and Marty, 1997; Bekkers et al., 1990; Forti et al., 1997; Murphy et al., 1995; Silver et al., 1996; McAllister and Stevens, 2000). However, such fluctuations have not been quantitatively analyzed. Similarly, nearly nothing is known about the variation in the rate of transmitter clearance from the cleft, and it is uncertain whether such a variation would result in a corresponding variability in PSC decay kinetics. Most studies have concentrated on analyzing the fluctuation of the peak amplitude of PSCs recorded under voltage-clamp, but variation in their decay is an equally important contributor to the variance of quantal charge transfer. To investigate this latter process, we combined electrophysiological, pharmacological, and modeling approaches to assess the contribution of fluctuations in the spatiotemporal profile of GABA in the synaptic cleft to the observed postsynaptic response variation.

Received for publication 13 September 2000 and in final form 11 December 2000.

Address reprint requests to Dr. Istvan Mody, Dept. of Neurology RNRC 3-155, Reed Neurological Research Center, UCLA School of Medicine, 710 Westwood Plaza, Los Angeles, CA 90095-1769. Tel.: 310-206-4481; Fax: 310-825-0033; E-mail: mody@ucla.edu.

Zoltan Nusser's present address is Institute of Experimental Medicine, Hungarian Academy of Sciences, 43 Szigony Street, 1083 Budapest, Hungary.

0006-3495/01/03/1251/11 $2.00

METHODS

Slice preparation and electrophysiological recordings

Sixteen- to sixty-day-old (P16-P60, 21.8 ± 9.7 (mean ± SD)) C57Black6 mice (n = 23) were anesthetized with halothane before decapitation in accordance with the guidelines of the UCLA Office for Protection of

Research Subjects. The brains were then removed and placed into an ice-cold artificial cerebrospinal fluid (ACSF) containing (in mM): 126 NaCl, 2.5 KCl, 2 $CaCl_2$, 2 $MgCl_2$, 1.25 NaH_2PO_4, 26 NaHCO3, 10 D-glucose, pH = 7.3 when bubbled with 95% O_2 and 5% CO_2. The visual cortex, cerebellum, or olfactory bulb was glued to a platform and 300-μm-thick sagittal (olfactory bulb, cerebellum) or coronal (visual cortex) slices were cut with a Vibratome (Lancer Series 1000) or Leica VT1000S. The slices were stored at 32°C in a holding chamber until transferred to the recording chamber. During recording, the slices were continuously perfused with 34°C ACSF containing 3–5 mM kynurenic acid and 1 μM tetrodotoxin as described earlier (Nusser et al., 1999b). All recordings were made from the somata of visually identified neurons (Zeiss Axioscope IR-DIC videomicroscopy, 40× water immersion objective) with an Axopatch 200B amplifier (Axon Instruments, Foster City, CA). Patch electrodes were filled with a solution containing (in mM): 140 CsCl, 4 NaCl, 1 $MgCl_2$, 10 Hepes, 0.05 EGTA, 2 Mg-ATP, and 0.4 Mg-GTP. All solutions were titrated to a pH of 7.25 and an osmolarity of 280–290 mOsmol. The resistance of the electrodes was between 3–8 MΩ when filled with pipette solution. Series resistance and whole-cell capacitance were estimated by compensating the fast current transients evoked at the onset and offset of 8 ms 5 mV voltage-command steps. We analyzed one to two minutes of recordings during which there was no change in the series resistance. The series resistance remaining after 75–80% compensation (with 7–8 μs lag values) was 3.2 ± 1.2 MΩ for layer2/3 pyramidal cells, 3.6 ± 1.0 MΩ for cerebellar interneurons, and 4.0 ± 1.1 MΩ for olfactory granule cells. All data are expressed as mean ± SD.

Solutions and drugs

Kynurenic acid and tetrodotoxin were purchased from Sigma and Calbiochem (La Jolla, CA), respectively. α-Latrotoxin (Alomone Labs., Jerusalem, Israel) was used at a final concentration of 200 nM. Microcystin-LR (Calbiochem) was first prepared as a 20 mM stock solution in DMSO, which was diluted 1000 times in the intracellular solution, resulting in a final concentration of 20 μM microcystin-LR and 0.1% DMSO in the intracellular solution. NO711 was purchased from RBI (Natick, MA) and was used at a final concentration of 2–5 μM.

Data analysis

All recordings were low-pass filtered at 2 kHz and on-line digitized at 20 kHz as described earlier (Nusser et al., 1999b). An in-house data acquisition and analysis software (written in LabView, National Instruments, Austin, TX) was used to measure the amplitudes, 10–90% rise times, 67% decay times, and charge transferred by mIPSCs. The decay of the averaged currents was fitted with a single or the sum of two exponential functions. The weighted decay time from the exponential fit ($\tau_{w(f)}$) was calculated as $\tau_{w(f)} = \tau_1 \cdot A_1 + \tau_2 \cdot (1 - A_1)$, where τ_1 and τ_2 are the fast and slow decay time constants, respectively, and A_1 is the contribution of the first exponential to the amplitude. The weighted decay time constant from the area ($\tau_{w(a)}$) was calculated by dividing the area of each mIPSC by its peak amplitude. Peak-scaled nonstationary fluctuation analysis was carried out with the same software, similarly to that described previously (De Koninck and Mody, 1994). Briefly, the averaged synaptic currents were binned into a user-defined number of bins (usually 20). Each individual mIPSC was scaled with a scaling factor to the peak of the averaged mIPSC, and the mean current (I) and the variance (σ^2) was calculated for each bin. Subsequently, the mean current and the variance have been scaled back with the scaling factor and the square of the scaling factor, respectively. The mean of the individual variances was then calculated and plotted against the mean current. This plot was fitted with the following equation using Origin (Microcal Software Inc., Northampton, MA).

$$\sigma^2 = -i \cdot I + 1/N_p \cdot I^2$$

to estimate the weighted mean single channel current (i) and the number of channels open at the peak of the averaged synaptic current (N_p).

Modeling of synaptic currents

Single channels were modeled with MatLab (MathWorks Inc., Natick, MA) using a Q-matrix algorithm (Colquhoun and Hawkes, 1995) according to a seven-state model (Jones and Westbrook, 1995) and the rate constants given in Fig. 5. Single-channel traces (25–40 ms long) were generated with a dt of 0.05 ms and an i of 2.5 pA, with an additional open channel Gaussian noise of 0.125 pA. Thirty to three-hundred channels were summed to generate a given IPSC and a Gaussian noise of 3–5 pA SD was added to resemble the baseline noise of the recorded IPSCs. A simulation session consisted of generating 50–100 PSCs. The cleft GABA concentration was modeled as an instantaneous rising function to $peak_{[GABA]}$ from which it decayed with either a single ($\tau_{[GABA]}$) or two ($\tau_{1[GABA]}$ = 0.1 ms; 87% share, and $\tau_{2[GABA]}$ = 2.1 ms) exponential functions. For each PSC, the $peak_{[GABA]}$ and $\tau_{[GABA]}$ could be individually set and they could be varied with an SD specified by the user. The simulated PSCs were analyzed using the same software as that used for the recorded mIPSCs.

RESULTS

First we used whole-cell patch-clamp recordings of mIPSCs from layer2/3 pyramidal cells of mouse visual cortex to examine the variability in the quantal synaptic charge transfer (Figs. 1 and 2 *D*). As dendritic filtering distorts fast synaptic currents and because the rise times, amplitudes, and decays of synaptic currents are considerably affected by voltage- and space-clamp errors, we only analyzed mIPSCs with very fast 10–90% rise times. It has been demonstrated (Bier et al., 1996; Borst et al., 1994; Brickley et al., 1996) that mIPSCs recorded from electrotonically compact cells

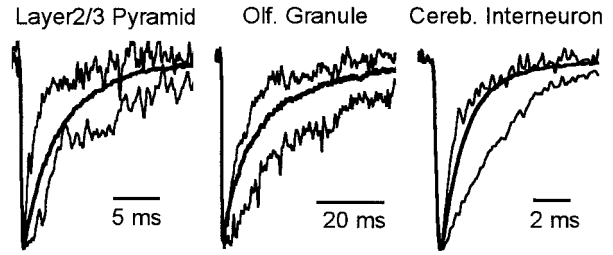

FIGURE 1 Large variability in the decay time course of mIPSCs recorded in three cell types. In a layer2/3 pyramidal cell of the visual cortex, rapidly and slowly decaying mIPSCs are shown (*thin traces*) in comparison with the averaged synaptic current (*thick trace*). The amplitudes of the synaptic currents have been normalized. The weighted decay time of the slowly decaying current ($\tau_{w(a)}$ = 8.1 ms) is more than five times slower than that of the rapidly decaying current ($\tau_{w(a)}$ = 1.6 ms), compared to the $\tau_{w(a)}$ of 4.8 ms for the averaged current. In granule cells of the olfactory bulb a similar variability in the decay of mIPSCs is detected, although the average $\tau_{w(a)}$ (14.8 ms; *thick trace*) was approximately three times larger than in layer2/3 pyramidal cells. The rapidly decaying current has a $\tau_{w(a)}$ that is three times faster than that of the slowly decaying PSC (9.3 vs. 27.0 ms). In cerebellar interneurons, the decay of mIPSCs also shows a remarkable variability (rapidly decaying IPSC: $\tau_{w(a)}$ = 1.9 ms vs. slowly decaying current: $\tau_{w(a)}$ = 4.0 ms), although they express only a single $GABA_A$ receptor subtype. Note the very fast decay time course of the averaged PSC ($\tau_{w(a)}$ = 2.1 ms, thick trace) in these cells.

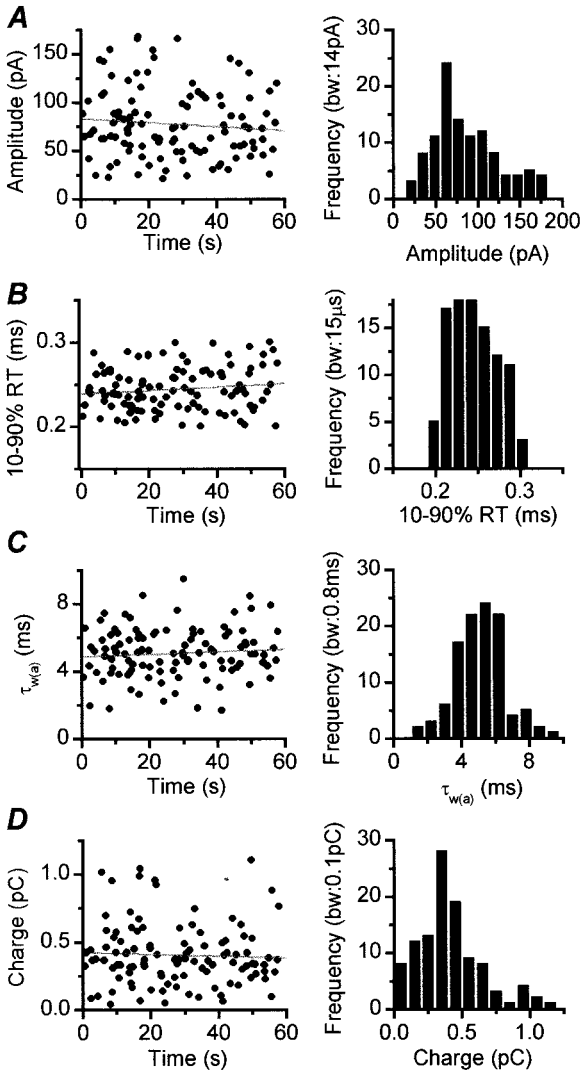

FIGURE 2 Variability in mIPSC parameters recorded in a neocortical layer2/3 pyramidal cell. *Left panels:* stability of the amplitude (*A*), 10–90% rise time (*B*), $\tau_{w(a)}$ (*C*), and transferred charge (*D*) of the synaptic currents during the 1-min recording period (linear regression fit: *A*, $R = -0.09$, $p = 0.34$, *t*-test; *B*, $R = 0.13$, $p = 0.17$; *C*, $R = 0.08$, $p = 0.39$; *D*, $R = -0.04$, $p = 0.63$). *Right panels:* distribution of mIPSC amplitudes (*A*; mean = 78 pA and CV = 0.46), 10–90% rise times (*B*; mean = 0.24 ms and CV = 0.1), $\tau_{w(a)}$ (*C*; mean = 5.1 ms and CV = 0.29), and transferred charges (*D*; mean = 406 fC and CV = 0.57). *bw* denotes bin width.

have 10–90% rise times of <500 μs. Thus, restricting our analysis to mIPSCs with 10–90% rise times ranging from 200 to 300 μs (Fig. 2 *B*) should allow us to focus on synaptic currents originating from equally well-clamped synapses. Special care was taken to analyze short periods of recordings, during which no change in the series resistance and the measured synaptic parameters was observed (Fig. 2). Thus, run-downs or run-ups during the recordings did not contribute to the variability of the synaptic parameters. In layer2/3 pyramidal cells there was a remarkable variability (coefficient of variation (CV) = 0.32 ± 0.03, $n = 6$ cells) in the weighted decay time constant of mIPSCs (Fig. 2 *C*), contributing ~40% to the variance observed in the synaptic charge transfer (Fig. 2 *D*, CV = 0.5 ± 0.06). The remaining ~60% variance was due to the amplitude variability (Fig. 2 *A*; CV = 0.41 ± 0.03; note that variances, and not CVs, add linearly). We tested whether such pronounced variability in the decay times is only present in this cell type, where IPSCs have a relatively fast decay time course (weighted decay time calculated from the area ($\tau_{w(a)}$): 5.8 ± 0.9 ms at 34°C, $n = 6$ cells). In granule cells of the main olfactory bulb, having a much slower IPSC $\tau_{w(a)}$ (14.0 ± 4.3 ms; Nusser et al., 1999b), a very similar variation in the mIPSC decay times was observed (Fig. 1; CV = 0.28 ± 0.09, $n = 4$ cells). Both layer2/3 pyramidal cells and olfactory granule cells express a large number of $GABA_A$ receptor subunits (Fritschy and Mohler, 1995; Persohn et al., 1992; Wisden et al., 1992), which assemble into several receptor subtypes. Therefore, the observed decay variability may originate from synapses containing different $GABA_A$ receptor subtypes (Fritschy et al., 1998; Koulen et al., 1996; Nusser et al., 1996), producing distinct PSC kinetics.

To circumvent this problem, the variability in mIPSC decay times was analyzed in GABAergic interneurons (stellate/basket cells) of the molecular layer of the cerebellar cortex, as they are likely to express only a single receptor subtype with $\alpha_1\beta_2\gamma_2$ subunit composition (Nusser et al., 1999a, b; Persohn et al., 1992) and are amenable to high-quality patch-clamp recordings (Auger and Marty, 1997; Llano and Gerschenfeld, 1993; Nusser et al., 1997). In these cells, the variability in the decay of synaptic currents (Figs. 1 and 3 *C*; $\tau_{w(a)} = 3.2 \pm 0.9$ ms; CV = 0.26 ± 0.07, $n = 15$ cells) was comparable to that recorded in layer2/3 pyramidal cells and olfactory granule cells. However, the decay variability contributed only 22% to the variability of the synaptic charge transfer (Fig. 3 *D*; CV = 0.55 ± 0.1). This is a reflection of the very pronounced mIPSC amplitude variation in these cells (Auger and Marty, 1997; Llano and Gerschenfeld, 1993; Nusser et al., 1997). The CV of the peak amplitude of mIPSCs was 0.53 ± 0.11 (Fig. 3 *A*) when only mIPSCs with 10–90% rise times of 200–300 μs were analyzed (Fig. 3 *B*). The major contributor to this large-amplitude variability is the large variation in the postsynaptic receptor number between synapses (Nusser et al., 1997), but at large synapses where postsynaptic $GABA_A$ receptors are not fully occupied, some variation also originates from the fluctuation in the peak transmitter concentration. The variability in the decay of small amplitude synaptic currents was found to be consistently larger than that of large-amplitude IPSCs in every cell type studied (e.g., Fig. 3 *E*). For cerebellar interneurons, the CV of the $\tau_{w(a)}$ for the smaller 50% of mIPSC amplitudes (CV = 0.30 ± 0.08) was almost twice as large ($p < 0.0001$, paired *t*-test, $n = 14$ cells) as that for the large mIPSCs (CV = 0.16 ± 0.04).

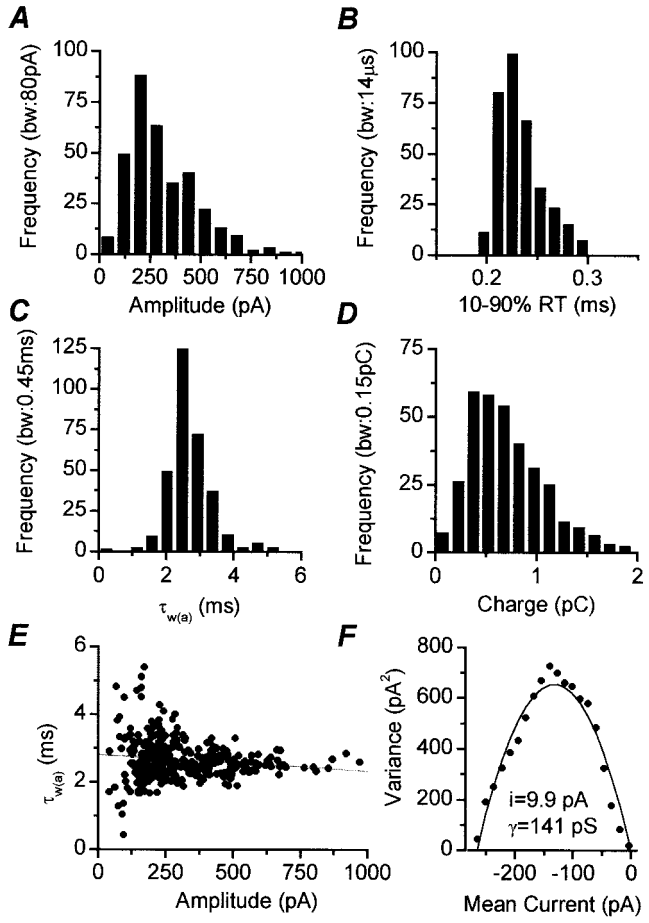

FIGURE 3 Heterogeneous mIPSC properties in a cerebellar interneuron. (*A*) Miniature IPSCs have a positively skewed amplitude distribution with a mean of 271 pA and a CV of 0.56. (*B*) Miniature currents with 10–90% rise times between 0.2–0.3 ms were selected for the analysis. The mean 10–90% rise time is 0.23 ms with an SD of 0.02. (*C*) The weighted decay time of mIPSCs showed 23% variability in this cell (mean = 2.7 ms; range: 0.4–5.4 ms). A similar decay variability is found if calculated from the 67% decay time (CV = 0.25, mean = 2.1 ms). (*D*) The charge transferred by mIPSCs shows a positively skewed distribution with a mean of 713 fC and a CV of 0.55. (*E*) Scatter plot of mIPSC weighted decay times versus peak amplitudes shows that the variability in the decay of small amplitude synaptic currents is much larger than that for large amplitude PSCs. The gray line indicates a linear fit to the data ($R = -0.11$, $p > 0.01$) (*F*) A parabolic relationship is seen between the mean current and peak-scaled variance. The parabolic fit provided an estimated weighted mean single-channel current of 9.9 pA, corresponding to a channel conductance of 141 pS (at −70 mV).

As phosphorylation by cAMP-dependent protein kinase prolongs the decay time of mIPSCs in cerebellar stellate/basket cells (Nusser et al., 1999b), a differential degree of phosphorylation at distinct sites could, in theory, account for some of the observed decay variability. To test the extent to which a differential phosphorylation of $GABA_A$ receptors at distinct sites contributes to the decay variability, we included 20 μM microcystin, a protein phosphatase 1/2A inhibitor, into the patch electrode and recorded mIPSCs from cerebellar stellate/basket cells. Blocking phosphatase activity results in a phosphorylation of the $GABA_A$ receptors or some associated proteins and a consequent slowing of the decay time course (Nusser et al., 1999b), but there was no significant ($p = 0.45$, Mann-Whitney U test) reduction in the CV of the decay times (CV = 0.23 ± 0.05, n = 5 cells). Another possible mechanism responsible for the observed decay variability is a differential contribution of GABA transporters to the clearance of GABA at distinct synapses on a single cell. To test this possibility, we examined the effect of 2–5 μM NO711, a selective GABA uptake inhibitor (Suzdak et al., 1992), on the decay variability. The application of NO711 resulted in a 56% prolongation of $\tau_{w(a)}$ in cerebellar interneurons (from 2.5 ± 0.6 to 3.9 ± 1.0 ms, $p < 0.02$, paired t-test). This was due to a similar prolongation of the slowly and rapidly decaying mIPSCs, indicating that all sites generating PSCs were affected by the uptake blocker. However, there was no significant ($p = 0.18$, paired t-test) change in the CV (NO711: 0.34 ± 0.02 vs. control: 0.30 ± 0.08, $n = 4$ cells) of $\tau_{w(a)}$, demonstrating that unequal GABA uptake is unlikely to be responsible for the variation in mIPSC decay times.

Variations in the decay of PSCs can be analyzed with peak-scaled nonstationary fluctuation analysis (psNSFA) to estimate the weighted mean single channel current (i) and the number of channels open at the peak of the averaged synaptic current (N_p; De Koninck and Mody, 1994; Traynelis and Jaramillo, 1998; Traynelis et al., 1993). This analysis relies on the critical assumption that all variance in the decay of the PSCs originates from the stochastic behavior of a homogeneous population of channels. We applied this analysis to every mIPSC with 200–300 μs 10–90% rise times recorded in cerebellar interneurons and found parabolic relationships between the mean current and the variance, as shown for a representative cell in Fig. 3 *F*. Applying psNSFA in 10 cells resulted in an i estimate of 5.1 ± 2.2 pA, corresponding to 73 ± 31 pS weighted mean single channel conductance (γ) at −70 mV. To ascertain that a significant correlation between the amplitude and $\tau_{w(a)}$ of the IPSCs did not result in an erroneous estimation of i, we analyzed the relationships between these parameters in 10 cells. In 8 of 10 cells there was no significant correlation between the amplitude and $\tau_{w(a)}$ (e.g., Fig. 3 *E*) and psNSFA yielded an i of 5.2 ± 2.1 pA, corresponding to a γ of 74 ± 30 pS. In one cell we found a significant positive correlation (i = 7.3 pA) and in another cell a significant negative correlation (i = 2.2 pA) between amplitude and $\tau_{w(a)}$. Thus, 74 pS channels would be required to describe the variance in the decay of these mIPSCs. Are there any 74 pS channels in these cells? The largest conductance state of $GABA_A$ receptors with $\alpha_1\beta_2\gamma_2$ subunit composition is 28 pS (Angelotti and Macdonald, 1993; Brickley et al., 1999), which is in excellent agreement with the channel conductance (28 pS; both recorded at room temperature) of $GABA_A$ receptors excised from cerebellar stellate/basket cells (Llano and

Gerschenfeld, 1993). Increasing the temperature from ~22 to ~35°C results in an ~25% increase in the channel conductance of $GABA_A$ receptors (from 26 to 32 pS in layer5 pyramidal cells and from 22 to 28 pS in dentate granule cells; De Koninck and Mody, 1994; Nusser et al., 1998; Perrais and Ropert, 1999). Thus the 28 pS conductance recorded at room temperature would correspond to 35 pS at 35°C, used in the present study. This value is still less than half of the 74 pS estimate from psNSFA. Thus, the most parsimonious explanation of this result is that the basic assumptions of psNSFA are not fulfilled. Namely, not all variability in IPSC decay originates from stochastic channel behavior. What could be the source of the additional variability? The most likely possibility is that the spatiotemporal profile of the GABA concentration in the synaptic cleft varies either between synapses or even at a single synapse from trial to trial.

To estimate the contribution of inter- and intra-site variability to the total mIPSC decay variability, we used 200 nM α-Latrotoxin to identify single release sites as described by Auger and Marty (1997). In most of our recorded cells the mean mIPSC frequency was >5 Hz, and in these cells bursts caused by α-Latrotoxin could not be unequivocally identified. To overcome this difficulty we chose cells close to the surface of the slice, where the mean IPSC frequency was low. In one-third (three of nine) of such cells, we could identify single release sites. Miniature PSCs recorded from such a cell are shown in Fig. 4, *A* and *C*. During a 60-s recording we plotted the amplitude of every mIPSC (Fig. 4 *B*). According to the graph, there are two distinct populations of mIPSC amplitudes. The amplitude distribution of each population could be well-described by a single Gaussian (Fig. 4 *D*), indicating that every mIPSC within a population originates from a single site. In good agreement with the work of Auger and Marty (1997), the variability in the peaks of small mIPSCs (CV = 0.096) is much less than that in the peaks of large PSCs (CV = 0.26; Fig. 4, *C* and *D*). The CV of 0.096 in the peak amplitude of small mIPSCs indicates a peak open probability (P_o) of 0.82, whereas an upper limit of 0.6 can be calculated for the P_o at the synapse generating the large PSCs (calculated as in Silver et al., 1996). The variability in the peak amplitude of small PSCs could be described by the stochastic behavior of ~25–30 channels (assuming a channel conductance of ~35 pS). However, to account for the peak amplitude variability of the large mIPSCs, a significant fluctuation in the peak GABA concentrations is required (see below).

The variability in the decay of mIPSCs at these two sites showed a different picture (Fig. 4 *E*). The CV of the $\tau_{w(a)}$ of the "large" mIPSCs was only 0.092, whereas that for the "small" mIPSCs was 0.23. The average CV of $\tau_{w(a)}$ for the three "large" single sites (>445 pA) identified in this study was 0.08 ± 0.01, whereas at the three "small" release sites (<140 pA) it was 0.33 ± 0.1. Using psNSFA at these synapses, a γ of 36 pS was determined from the variability in the decay of "large" mIPSCs (Fig. 4 *F*), but 67-pS channels would be required to account for the decay variability of the "small" mIPSCs. In the second and third cells we have identified one and three single sites, respectively. The average γ for the "large" single sites was 36.1 ± 1 pS, whereas it was 75 ± 16.8 pS at the "small" release sites. For IPSCs recorded at three "large" single sites and at two of three "small" single sites, no significant correlation was observed between the amplitude and the $\tau_{w(a)}$. Despite this lack of correlation, in these two recordings of "small" events the estimated γ were 67 and 96 pS. As calculated above, the γ of the $GABA_A$ receptors ($\alpha_1\beta_2\gamma_2$) in cerebellar stellate/basket cells is predicted to be ~35 pS at physiological temperatures. Considering that only one type of channel is present at both sites generating either "large" or "small" PSCs, such channels account for all variability in the decay of "large" mIPSCs, but a significant additional source of variability must exist at the sites generating "small" PSCs. As we could not directly monitor the synaptic GABA transients and we had no direct measure for its trial-to-trial fluctuation, we turned to computer simulations to predict the required variability in the synaptic GABA concentration profile to account for the measured variability in mIPSCs.

We have used a seven-state model of $GABA_A$ receptors (Jones and Westbrook, 1995) and optimized the rate constants (least-square method) to provide an adequate fit to an averaged mIPSC recorded in a cerebellar interneuron (Fig. 5 *A*). In our simulations, instead of using the probability density function of the open states, individual PSCs were generated as a sum of an arbitrary number of channels, allowing the characterization of the variability in the peak and decay of the simulated PSCs. In an initial set of simulations, a single-exponential function was used to describe the agonist clearance rate ($\tau_{[GABA]}$; Glavinovic, 1999; Mozrzymas et al., 1999). Both the peak GABA concentration ($peak_{[GABA]}$) and the $\tau_{[GABA]}$ could be varied from one IPSC to the next with a user-defined SD around a mean. Fig. 5 *B* demonstrates the effect of $\tau_{[GABA]}$ on the $peak_{[GABA]}$ versus peak IPSC open probability (P_o) curves. With $\tau_{[GABA]}$ <0.1 ms, very high concentrations of GABA (>20 mM) were needed to obtain a P_o of 0.8 (characterizing the small release sites), which is very unlikely to occur (Jones and Westbrook, 1995; Maconochie et al., 1994; Mozrzymas et al., 1999; Perrais and Ropert, 1999). However, with $\tau_{[GABA]}$ >1 ms, a $peak_{[GABA]}$ of ~0.08 mM was already sufficient to produce PSCs with P_o of 0.5 (characterizing the large single sites), but the rise times of these PSCs were too slow (>1.5 ms) and therefore, incompatible with our experimental observations. With $\tau_{[GABA]}$ = 0.3 ms, a $peak_{[GABA]}$ of 1 mM already produced saturation of the postsynaptic receptors, and a $peak_{[GABA]}$ of 0.2 mM resulted in a peak PSC P_o of 0.5 with a 10–90% rise time (<0.3 ms) compatible with the experimental data. Therefore, we used a mean $\tau_{[GABA]}$ of 0.3 ms and a mean $peak_{[GABA]}$ of 1 mM to investigate the degree of variability in the synaptic

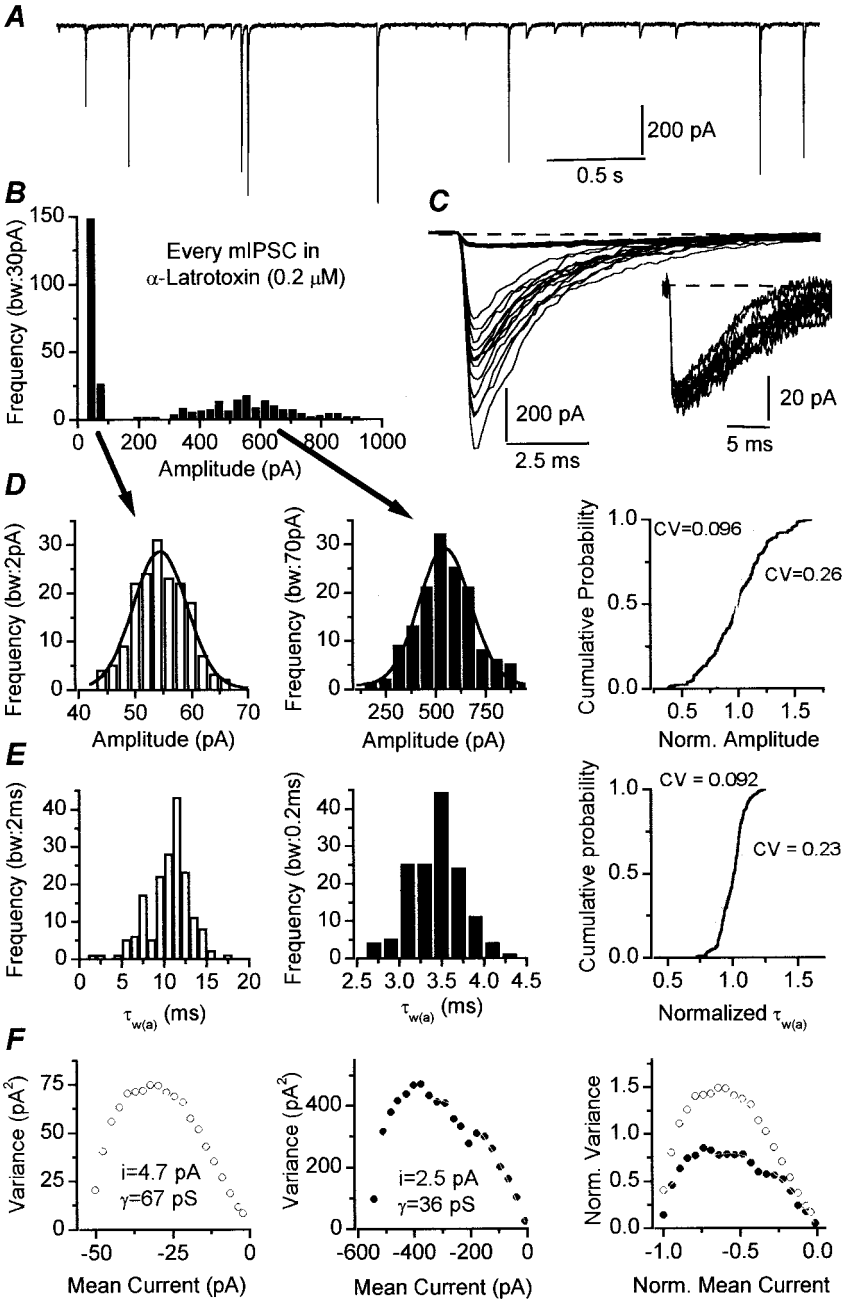

FIGURE 4 Characterization of mIPSC decay variability at single release sites in a cerebellar interneuron. (*A*) Four seconds of continuous recordings in 0.2 μM α-Latrotoxin. (*B*) Amplitude histogram of every mIPSC recorded within a 60-s period in the presence of 0.2 μM α-Latrotoxin shows two non-overlapping populations of events. Both populations are re-binned and re-plotted in *D*. (*C*) Twenty-four consecutive mIPSCs demonstrate that there is a much smaller variability in the peak amplitude of the small currents than that of the large PSCs. The inset shows the small IPSCs on expanded scales. (*D*) The amplitude distributions of both the small (*left panel*) and the large (*middle panel*) events are each adequately fitted by a single Gaussian function. This indicates that both types of events originate from single sites. Cumulative probability plot (*right panel*) of normalized amplitudes of the small and large PSCs shows a much larger variability in the peak amplitude of the large (*black line*; CV = 0.23) than the small (*gray line*; CV = 0.096) events. (*E*) Distributions of $\tau_{w(a)}$ of the small (*left panel*) and large (*middle panel*) mIPSCs. Note that the mean $\tau_{w(a)}$ of the small currents is larger than that of the large IPSCs (10.6 $\pm$ 2.5 vs. 3.4 $\pm$ 0.3). Cumulative probability plot of the normalized weighted decay times (*right panel*) demonstrates the variability in the decay of the small mIPSCs to be much larger (*gray line*; CV = 0.23) than that for the large PSCs (*black line*; CV = 0.092). (*F*) Peak-scaled non-stationary fluctuation analysis of the small (*left panel*) and large (*middle panel*) PSCs yields a weighted mean single-channel current (*i*) of 4.7 and 2.5 pA, respectively, corresponding to weighted mean single-channel conductance (γ) of 67 and 36 pS. Superimposed normalized mean current versus normalized variance plots (*right panel*) demonstrate a nearly two-times larger variance in the decay of the small PSCs compared to that of the large currents.

GABA transients needed to describe the decay variability in the "small" single-site mIPSCs. First, we examined whether fluctuations in the peak GABA concentration could account for the observed IPSC decay variability. Increasing the mean $\text{peak}_{[GABA]}$ from 0.1 to 10 mM resulted in no significant change in the decay of PSCs (Fig. 6 *A*). Indeed, when a CV of $\text{peak}_{[GABA]}$ of 0.54 was included in a single simulation, no correlation between the $\text{peak}_{[GABA]}$ and $\tau_{w(a)}$ was observed (Fig. 6 *B*). Thus, variability in the peak GABA concentration could not account for the variation in the decay of the synaptic currents when a single exponential function ($\tau_{[GABA]}$ = 0.3 ms) was used to describe the synaptic GABA clearance rate (Fig. 6 *C*). In our next set of simulations we tested whether variability in the GABA clearance rate could be responsible for the observed IPSC decay variability. When the mean $\tau_{[GABA]}$ was increased from 0.1 to 6 ms, a significant prolongation of the $\tau_{w(a)}$ was observed (Fig. 6 *D*). Indeed, when variability in $\tau_{[GABA]}$ was included within a single simulation, an increased $\tau_{[GABA]}$ resulted in a significant prolongation of $\tau_{w(a)}$ (Fig. 6 *E*). CV analysis (Fig. 6 *F*) demonstrated that a CV of $\tau_{[GABA]}$ of >55% is necessary to describe the experimentally observed IPSC decay variability. In simulations, with no variability in the $\tau_{[GABA]}$, psNSFA reliably reproduced the single channel

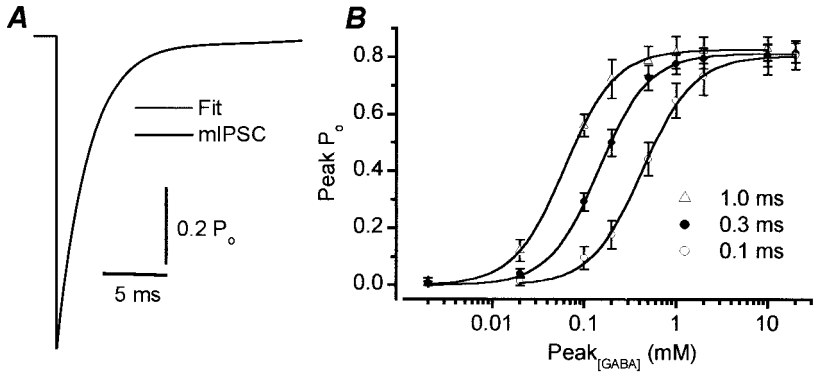

FIGURE 5 IPSCs generated with a seven-state kinetic model. (*A*) Superimposed traces of an averaged stellate cell mIPSC (*gray trace*; peak normalized to $P_o = 0.8$; $\tau_1 = 1.9$ ms (86%), $\tau_2 = 7.9$ ms; $\tau_{w(f)} = 2.7$ ms; $\tau_{w(a)} = 2.7$ ms) and a simulated PSC (*black trace*; $\tau_1 = 2.2$ ms (92%), $\tau_2 = 10.8$ ms; $\tau_{w(f)} = 2.9$ ms; $\tau_{w(a)} = 2.8$ ms) with the following rate constants using the seven-state model of $GABA_A$ receptors: $k_{on} = 50\ ms^{-1}\ mM^{-1}$; $k_{off} = 2.36\ ms^{-1}$; $\beta_1 = 0.20\ ms^{-1}$; $\alpha_1 = 1.11\ ms^{-1}$; $\beta_2 = 11.4\ ms^{-1}$; $\alpha_2 = 1.5\ ms^{-1}$; $d_1 = 0.013\ ms^{-1}$; $r_1 = 0.00013\ ms^{-1}$; $d_2 = 1.08\ ms^{-1}$; $r_2 = 0.13\ ms^{-1}$. The peak GABA concentration was 1 mM and the duration (square pulse) of GABA was 0.3 ms. (*B*) Peak GABA concentration ($peak_{[GABA]}$) versus peak IPSC open probability (peak P_o) plots for three different GABA clearance rates ($\tau_{[GABA]} = 1$ ms (*open triangle*), 0.3 ms (*filled circle*), and 0.1 ms (*open circle*)).

conductance of the channels ($i_{estimated}/i_{real} = 1.04$); however, including a small additional variability in $\tau_{[GABA]}$ (17–44%) already resulted in a significant deviation of the estimated single channel current ($i_{estimated}/i_{real} = 1.26$). When the CV of $\tau_{[GABA]}$ was increased to >50%, a very robust deviation in the estimated i was observed ($i_{estimated}/i_{real} = 1.9$; Fig. 7 *C*). We also tested how changing the mean value of $\tau_{[GABA]}$ (from 0.1 to 1 ms) influences the $i_{estimated}/i_{real}$ ratio. Although the decay times of the PSCs were strongly influenced by increasing the $\tau_{[GABA]}$ within a simulation (Fig. 6 *E*) and between simulations (Fig. 6 *D*), the $i_{estimated}/i_{real}$ ratio remained virtually unchanged ($\tau_{[GABA]} = 0.1$ ms: $\tau_{w(a)} = 3.04 \pm 0.01$ ms and $i_{estimated}/i_{real} = 1.04$; $\tau_{[GABA]} = 1$ ms: $\tau_{w(a)} = 5.27 \pm 0.06$ ms and $i_{estimated}/i_{real} = 1.08$). Furthermore, within a given simulation session the amplitude of the simulated IPSCs was not correlated with the $\tau_{w(a)}$ (Fig. 7 *A*), and this finding was consistent across all 16 simulations (Fig. 7 *B*). Thus, changing the mean value of $\tau_{[GABA]}$ alone cannot account for our experimental observation of additional variability in PSC decay at small sites (Fig. 4 *E*), but a CV in the $\tau_{[GABA]}$ of >55% is necessary. In our simulations with a single exponential $\tau_{[GABA]}$, variation in the peak GABA concentration did not contribute to the IPSC decay variability. To test whether this also held true when GABA clearance was modeled with the sum of two exponential functions ($\tau_{1[GABA]} = 0.1$ ms (87%), $\tau_{2[GABA]} = 2.1$ ms; see Clements, 1996), we tested the effect of increasing mean $peak_{[GABA]}$ (0.1–10 mM) on the mean $\tau_{w(a)}$. Interestingly, in contrast to data obtained with a single-exponential GABA clearance, increasing $peak_{[GABA]}$ significantly prolonged the decay of PSCs (Fig. 6 *G*). Within a single simulation with a CV of $peak_{[GABA]}$ of 0.51, there was a significant positive correlation between the $peak_{[GABA]}$ and $\tau_{w(a)}$ (Fig. 6 *H*). The relationship between the CV of $peak_{[GABA]}$ and the CV of $\tau_{w(a)}$ (Fig. 6 *I*), when GABA clearance is approximated with two exponential functions, indicates that fluctuations in the peak GABA concentration can contribute to, but cannot fully account for, the variability in the IPSC decay in our simulations. In our experiments the CV of $\tau_{w(a)}$ at the small single site shown in Fig. 4 was 0.23, while the mean CV of $\tau_{w(a)}$ for the three small single sites was 0.33. These values are still larger than the maximum CV of $\tau_{w(a)}$ from our simulations (CV = 0.187 at a CV of $peak_{[GABA]} = 0.53$).

To address how much variation in the $peak_{[GABA]}$ is needed to characterize the fluctuation in the peak amplitude of the "large" single-site IPSCs we used a mean $\tau_{[GABA]}$ of 0.3 ms with no variability and a mean $peak_{[GABA]}$ of 0.2 mM to obtain an average peak IPSC P_o of 0.5. We found a steep, positive, linear correlation between the CV of the $peak_{[GABA]}$ and the CV of IPSC amplitude. As can be seen from Fig. 7 *D*, ~30% variability in the $peak_{[GABA]}$ is required to describe the amplitude fluctuation observed at large single sites.

DISCUSSION

We have identified a large variability in the decay of $GABA_A$ receptor-mediated IPSCs, contributing 20–40% to the total quantal charge variability. This variability was present in several cell types, including cerebellar interneurons, thought to express only a single subtype of $GABA_A$ receptor ($\alpha_1\beta_2\gamma_2$). In these cells, variability in $\tau_{w(a)}$ does not originate simply from differences in the PSCs decays generated at distinct synapses, as there is a significant trial-to-trial intra-site variability. This latter intra-site variation was significantly larger for small than for large IPSCs, possibly indicating different sources of variance in the decay of these two event types. The variance in the decay of large IPSCs

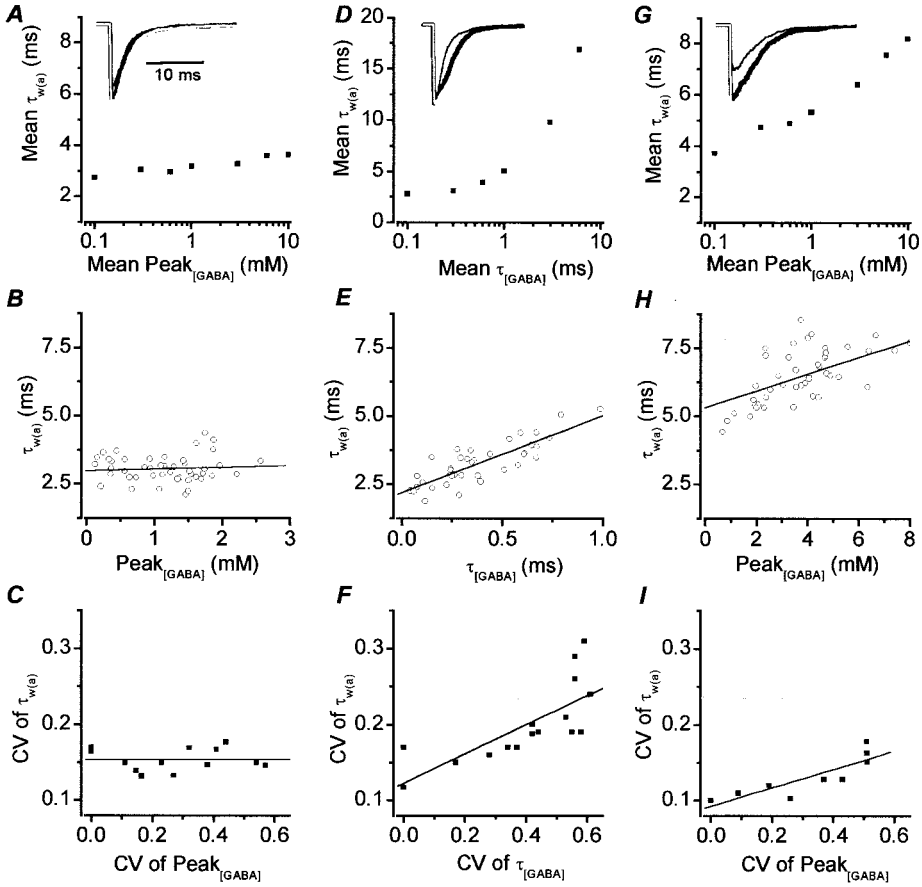

FIGURE 6 Predicting the variability in the synaptic GABA concentration profile. Simulations with either single (*A--F*) or double (*G--I*; $\tau_{1[GABA]} = 0.1$ ms (87%) and $\tau_{2[GABA]} = 2.1$ ms) exponential decays of the synaptic GABA concentration. (*A*) Increasing the mean peak$_{[GABA]}$ has no significant effect on the mean $\tau_{w(a)}$ when a single-exponential GABA clearance is present ($\tau_{[GABA]} = 0.3 \pm 0$ ms). The inset shows three averaged IPSCs generated with peak$_{[GABA]}$ of 0.3 ± 0 mM (*thin trace*), 1 ± 0 mM (*thick trace*), and 6 ± 0 mM (*gray trace*). (*B*) No significant ($R = 0.08$, $p = 0.57$) correlation exists between peak$_{[GABA]}$ and $\tau_{w(a)}$ within a single simulation (mean peak$_{[GABA]} = 1$ mM, CV of peak$_{[GABA]} = 0.54$). (*C*) Increasing the CV of peak$_{[GABA]}$ does not increase the CV of $\tau_{w(a)}$, demonstrating that variability in the peak GABA concentration cannot describe the experimentally observed IPSC decay variability (*dashed gray line*, as in Fig. 4 *E*) when the GABA clearance rate is modeled with a single exponential function ($\tau_{[GABA]} = 0.3 \pm 0$ ms). (*D*) Increasing the mean $\tau_{[GABA]}$ results in a prolongation of the mean $\tau_{w(a)}$ in simulations using a single exponential $\tau_{[GABA]}$ (mean peak$_{[GABA]} = 1 \pm 0$ mM). The inset shows three averaged IPSCs generated with $\tau_{[GABA]}$ of 0.3 ± 0 ms (*thin trace*), 1 ± 0 ms (*thick trace*), and 6 ± 0 ms (*gray trace*). (*E*) A significant positive correlation ($R = 0.83$; $p < 0.0001$, *t*-test) is found between $\tau_{[GABA]}$ (mean = 0.38 ms, CV = 0.60) and $\tau_{w(a)}$ of 50 simulated IPSC (same simulation as Fig. 7, *A* and *C*). (*F*) There is a significant ($R = 0.75$, $p < 0.001$) correlation between the CV of $\tau_{[GABA]}$ and the CV of $\tau_{w(a)}$, demonstrating that ~55% variability in the GABA clearance rate could account for the experimentally observed variability in $\tau_{w(a)}$ (*dashed gray line*). (*G*) When the GABA clearance rate is a double exponential, an increase in the peak$_{[GABA]}$ also results in a significant prolongation of the IPSC decay. *Inset:* averaged IPSCs generated with peak$_{[GABA]}$ of 0.3 ± 0 mM (*thin trace*), 1 ± 0 mM (*thick trace*), and 6 ± 0 mM (*gray trace*). (*H*) Within a single simulation (mean peak$_{[GABA]}$ = 3.9 mM, CV of peak$_{[GABA]} = 0.51$), higher peak$_{[GABA]}$ prolonged IPSC decay times ($R = 0.62$, $p < 0.001$). (*I*) An increase in the CV of peak$_{[GABA]}$ caused an enhancement of the CV of $\tau_{w(a)}$ when two exponentials are used to model the GABA clearance rate. However, the experimentally observed decay variability (*dashed gray line*) could not be fully accounted for by the peak$_{[GABA]}$ fluctuation.

could be fully accounted for by the stochastic behavior of channels with a chord conductance of 36 pS, in good agreement with the predicted value for the $\alpha_1\beta_2\gamma_2$ receptors at 35°C (35 pS; Brickley et al., 1999; Llano and Gerschenfeld, 1993; Perrais and Ropert, 1999). In our previous study using psNSFA (Nusser et al., 1997), we also arrived at a γ of 27 pS at "large" mIPSCs at room temperature, which would correspond to 34 pS at 35°C. In contrast, at synapses generating small PSCs, the erroneous estimate of single channel conductance (75 pS) suggests the presence of an additional source of variability. Modeling of PSCs required the incorporation of >55% variability in $\tau_{[GABA]}$ at release sites producing small PSCs (assuming single-exponential GABA clearance) or significant variability in both the peak GABA concentration and GABA clearance rate (assuming double-exponential GABA clearance). At these sites, fluctuation in the GABA concentration profile will not result in significant peak IPSC variability, as postsynaptic receptors seem to be fully occupied. In contrast, at large synapses where postsynaptic receptors are not fully occupied by the

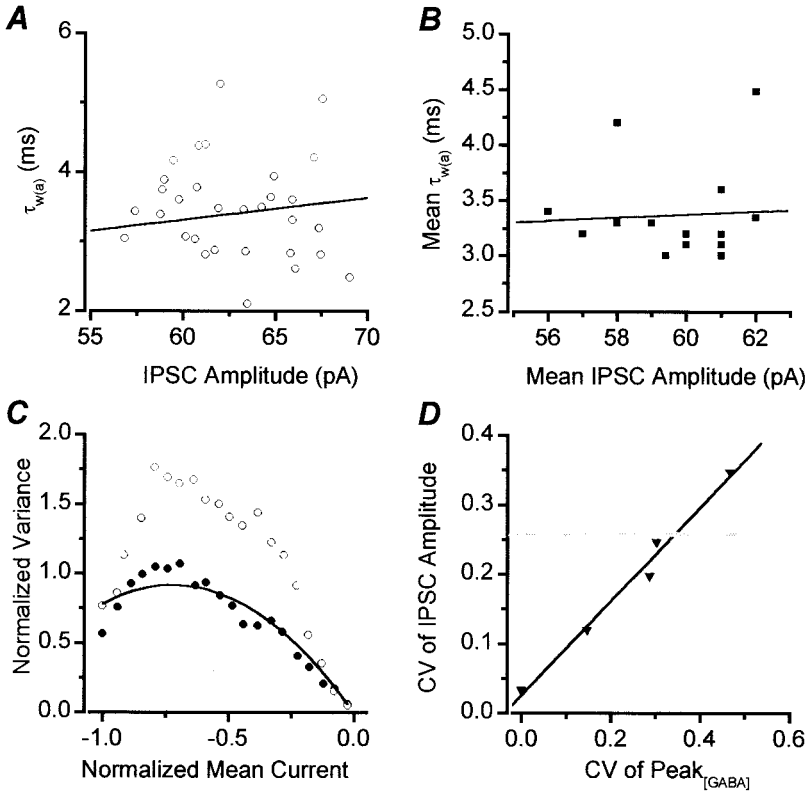

FIGURE 7 Effect of variable GABA concentrations and clearance rates on simulated mIPSCs. (*A* and *B*) IPSC amplitudes and decay times ($\tau_{w(a)}$) show no significant correlation either within a single simulation (*A*; $R = 0.41$, $p > 0.01$) or across all 16 simulations (*B*; $R = 0.06$, $p > 0.1$). (*C*) Normalized mean current versus normalized variance plot of 100 simulated IPSCs. Synaptic currents simulated with 60% CV in the $\tau_{[GABA]}$ (*open circles*, same as data shown in panel *A*) have approximately twice as much variance in their decay than those generated without any variability in $\tau_{[GABA]}$. (*D*) Effect of variability in the peak GABA concentration on the variation of simulated mIPSC amplitudes. A CV of ~30% in the peak$_{[GABA]}$ can account for the 26% variation (*gray dashed line*) in the amplitude of the large mIPSCs observed experimentally in cerebellar interneurons shown in Fig. 4 *D*. Linear fit to the data is shown by the black line (slope = 0.68; $R = 0.99$; $p < 0.0001$).

released transmitter, fluctuation in the synaptic GABA transients leads to a significant variability in PSC amplitudes.

Our results imply that the decay of $GABA_A$ receptor-mediated PSCs at certain synapses is not solely determined by the gating kinetics of the receptors (Faber et al., 1992; Jones and Westbrook, 1996). The decay is also affected by the spatiotemporal profile of GABA concentration, and therefore its trial-to-trial fluctuation will be reflected in the quantal charge transfer. We excluded the possibility that $GABA_A$ receptors are differentially regulated by PKA in stellate/basket cells, but other, yet unknown, regulatory mechanisms may alter the properties of postsynaptic receptors in a synapse-specific manner at a very fast time scale and may account for some of the observed IPSC decay variability. Nonstationary fluctuation analysis has been developed (De Koninck and Mody, 1994; Traynelis and Jaramillo, 1998; Traynelis et al., 1993) to gain insight into basic parameters (i, N_p, P_o) of ligand-gated channels underlying synaptic currents. This analysis relies on the critical assumption that all variance in the decay of the PSCs originates from the stochastic behavior of a homogeneous population of channels. The latter assumption is not fulfilled for non-NMDA receptor-mediated and $GABA_A$ receptor-mediated PSCs in most central neurons, as they express a large variety of receptor subunits (Fritschy and Mohler, 1995; Persohn et al., 1992; Sato et al., 1993; Wisden et al., 1992), which co-assemble into several receptor subtypes. At some synapses expressing multiple $GABA_A$ receptor subtypes, the weighted mean conductance estimated with psNSFA could correspond well with the actual conductance of synaptic receptors (Brickley et al., 1999). However, as shown here at different synapses, additional variance in the PSC decay caused by the variation in the spatiotemporal profile of the transmitter concentration will result in a considerable overestimation of γ. This is particularly relevant to experimental conditions where psNSFA is used to detect an increased variance in the decay of PSCs. Similarly to our results, Kurk et al. (1997) have also found that NSFA could result in an erroneous estimation of γ or N if postsynaptic receptors are exposed to a non-uniform transmitter concentration. Thus, these results point to the complexity inherent to the analysis of PSCs and call for caution when interpreting the results of NSFA of PSCs, in particular those with a large variance in their decays.

What is the mechanism underlying the large fluctuations in the spatiotemporal profile of the GABA concentration? A likely possibility is the multivesicular release of GABA described at cerebellar interneuronal synapses (Auger et al., 1998). The release of GABA from two or even more vesicles would not only result in an increase in the peak$_{[GABA]}$, but may also slow the $\tau_{[GABA]}$ (e.g., asynchronous release, reduced diffusion gradient). Several other mechanisms underlying the variation in the spatiotemporal profile of transmitter concentration could also be envisaged. The size of

synaptic vesicles shows a considerable variation in several synaptic boutons (Bekkers et al., 1990; Palay and Chan-Palay, 1974). If synaptic vesicles contain a uniform concentration of transmitter, the amount of transmitter released into the synaptic cleft will be proportional to the volume of the vesicle. However, the synaptic vesicles may also contain different transmitter concentrations resulting, for example, from the expression of different densities of vesicular transporters. The "kiss-and-run" hypothesis (Valtorta et al., 1990; Meldolesi, 1998) of vesicular fusion and a variation in the vesicle fusion time through an open pore with the plasma membrane (Glavinovic, 1999) may provide another possible mechanism for the variation of $\tau_{[GABA]}$. Changes in the volume of the synaptic cleft could, in theory, also result in differences in the spatiotemporal profile of GABA concentration.

An important task is to ascertain how the variable amounts of transmitter in the synaptic cleft will influence the peak$_{[GABA]}$ and the $\tau_{[GABA]}$ at synapses with distinct size and geometry. In cerebellar stellate/basket cells, we have previously identified (Nusser et al., 1997) that large mIPSCs originate from large synapses with many receptors, while small PSCs come from small synapses, containing fewer receptors. A 20- to 30-fold difference was found between the areas of the smallest and largest synapses, which translates into a similar difference in the volume of the cleft, as the cleft diameter was very similar at distinct sites. Detailed simulations based on 3D reconstructed neuronal tissue around synapses such as these will be required to estimate the transmitter diffusion inside and outside the synaptic cleft.

The contribution of variations in the spatiotemporal profile of the transmitter concentration to the variance in the decay of PSCs has important therapeutical consequences. Pharmacological manipulations that change the $\tau_{[GABA]}$ should influence the decay of IPSCs and consequently the synaptic charge transfer at some, but not necessarily all synapses. Indeed, blocking the GABA uptake with 2–5 μM NO711 resulted in a 56% prolongation of the decay of mIPSCs recorded from cerebellar stellate/basket cells. This drug should not influence the gating kinetics of the receptor, but is expected to alter the spatiotemporal profile of GABA concentration. This effect is by no means negligible, as clinically used anticonvulsants, antidepressants, sedative, and anxiolytic benzodiazepines (Nusser et al., 1997), and anesthetic barbiturates (Z. Nusser and I. Mody, unpublished observation), produce a similar prolongation of PSCs in these cells. Indeed, the GABA uptake inhibitor tiagabine has been recently introduced as a novel antiepileptic under the trade name Gabitril (Schachter, 1999). Our results imply that future drug design should exploit the variation in the spatiotemporal profile of the cleft GABA concentration to selectively alter GABAergic inhibition in a brain region- and synapse-specific manner.

We thank Drs. Mark Farrant and Thomas Otis for their comments on the manuscript and Dr. Thorsten Hodapp for creating the LabView analysis software.

This work was supported by NINDS Grant NS 30549 and the Coelho Endowment (to I.M.) and a Wellcome International Prize Traveling Research Fellowship (to Z.N.).

REFERENCES

Allen, C., and C. F. Stevens. 1994. An evaluation of causes for unreliability of synaptic transmission. *Proc. Natl. Acad. Sci. U.S.A.* 91:10380–10383.

Angelotti, T. P., and R. L. Macdonald. 1993. Assembly of GABA$_A$ receptor subunits: $\alpha1\beta1$ and $\alpha1\beta1\gamma2s$ subunits produce unique ion channels with dissimilar single-channel properties. *J. Neurosci.* 13: 1429–1440.

Auger, C., S. Kondo, and A. Marty. 1998. Multivesicular release at single functional synaptic sites in cerebellar stellate and basket cells. *J. Neurosci.* 18:4532–4547.

Auger, C., and A. Marty. 1997. Heterogeneity of functional synaptic parameters among single release sites. *Neuron.* 19:139–150.

Bekkers, J. M., G. B. Richerson, and C. F. Stevens. 1990. Origin of variability in quantal size in cultured hippocampal neurons and hippocampal slices. *Proc. Natl. Acad. Sci. U.S.A.* 87:5359–5362.

Bergles, D. E., J. S. Diamond, and C. E. Jahr. 1999. Clearance of glutamate inside the synapse and beyond. *Curr. Opin. Neurobiol.* 9:293–298.

Bier, M., K. S. Kits, and J. G. G. Borst. 1996. Relation between rise times and amplitudes of GABAergic postsynaptic currents. *J. Neurophysiol.* 75:1008–1012.

Borst, J. G. G., J. C. Lodder, and K. S. Kits. 1994. Large amplitude variability of GABAergic IPSCs in melanotropes from *Xenopus laevis*: evidence that quantal size differs between synapses. *J. Neurophysiol.* 71:639–655.

Brickley, S. G., S. G. Cull-Candy, and M. Farrant. 1996. Development of a tonic form of synaptic inhibition in rat cerebellar granule cells resulting from persistent activation of GABA$_A$ receptors. *J. Physiol. (Lond.).* 497:753–759.

Brickley, S. G., S. G. Cull-Candy, and M. Farrant. 1999. Single-channel properties of synaptic and extrasynaptic GABA$_A$ receptors suggest differential targeting of receptor subtypes. *J. Neurosci.* 19:2960–2973.

Clements, J. D. 1996. Transmitter timecourse in the synaptic cleft: its role in central synaptic function. *Trends Neurosci.* 19:163–171.

Clements, J. D., R. A. J. Lester, G. Tong, C. E. Jahr, and G. L. Westbrook. 1992. The time course of glutamate in the synaptic cleft. *Science.* 258:1498–1501.

Colquhoun, D., and A. G. Hawkes. 1995. A Q-matrix cookbook: how to write only one program to calculate the single-channel and macroscopic predictions for any kinetic mechanism. *In* Single-Channel Recording. B. Sakmann and E. Neher, editors. Plenum Press, New York. 589–633.

Colquhoun, D., P. Jonas, and B. Sakmann. 1992. Action of brief pulses of glutamate on AMPA/Kainate receptors in patches from different neurones of rat hippocampal slices. *J. Physiol. (Lond.).* 458:261–287.

De Koninck, Y., and I. Mody. 1994. Noise analysis of miniature IPSCs in adult rat brain slices: properties and modulation of synaptic GABA$_A$ receptor channels. *J. Neurophysiol.* 71:1318–1335.

del Castillo, J., and B. Katz. 1954. Quantal components of the end-plate potential. *J. Physiol. (Lond.).* 124:560–573.

Faber, D. S., W. S. Young, P. Legendre, and H. Korn. 1992. Intrinsic quantal variability due to stochastic properties of receptor-transmitter interactions. *Science.* 258:1494–1498.

Forti, L., M. Bossi, A. Bergamaschi, A. Villa, and A. Malgaroli. 1997. Loose-patch recordings of single quanta at individual hippocampal synapses. *Nature.* 388:874–878.

Fritschy, J.-M., and H. Mohler. 1995. GABA$_A$-receptor heterogeneity in the adult rat brain: differential regional and cellular distribution of seven major subunits. *J. Comp. Neurol.* 359:154–194.

Fritschy J.-M., O. Weinmann, A. Wenzel, and D. Benke. 1998. Synapse-specific localization of NMDA and $GABA_A$ receptor subunits revealed by antigen-retrieval immunohistochemistry. *J. Comp. Neurol.* 390: 194–210.

Glavinovic, M. I. 1999. Monte Carlo simulation of vesicular release, spatiotemporal distribution of glutamate in synaptic cleft, and generation of postsynaptic currents. *Pflugers Arch.* 437:462–470.

Jones, M. V., and G. L. Westbrook. 1995. Desensitized states prolong $GABA_A$ channel responses to brief agonist pulses. *Neuron.* 15:181–191.

Jones, M. V., and G. L. Westbrook. 1996. The impact of receptor desensitization on fast synaptic transmission. *Trends Neurosci.* 19:96–101.

Koulen, P., M. Sassoe-Pognetto, U. Grunert, and H. Wassle. 1996. Selective clustering of $GABA_A$ and glycine receptors in the mammalian retina. *J. Neurosci.* 16:2127–2140.

Kurk, P. J., H. Korn, and D. S. Faber. 1997. The effects of geometrical parameters on synaptic transmission: a Monte Carlo simulation study. *Biophys. J.* 73:2874–2890.

Lisman, J. E. 1997. Bursts as a unit of neural information: making unreliable synapses reliable. *Trends Neurosci.* 20:38–43.

Llano, I., and H. M. Gerschenfeld. 1993. Inhibitory synaptic currents in stellate cells of rat cerebellar slices. *J. Physiol. (Lond.).* 468:177–200.

Maconochie, D. J., J. M. Zempel, and J. H. Steinbach. 1994. How quickly can $GABA_A$ receptors open? *Neuron.* 12:61–71.

McAllister, A. K., and C. F. Stevens. 2000. Nonsaturation of AMPA and NMDA receptors at hippocampal synapses. *Proc. Natl. Acad. Sci. U.S.A.* 97:6173–6178.

Meldolesi, J. 1998. Regulated exocytosis in neurons and neurosecretory cells: structural events and expression competence. *J. Physiol. (Paris)* 92:119–121.

Mozrzymas, J. W., A. Barberis, K. Michalak, and E. Cherubini. 1999. Chlorpromazine inhibits miniature GABAergic currents by reducing the binding and by increasing the unbinding rate of $GABA_A$ receptors. *J. Neurosci.* 19:2474–2488.

Murphy, T. H., J. M. Baraban, and W. G. Wier. 1995. Mapping miniature synaptic currents to single synapses using calcium imaging reveals heterogeneity in postsynaptic output. *Neuron.* 15:159–168.

Nusser, Z., Z. Ahmad, V. Tretter, K. Fuchs, W. Wisden, W. Sieghart, and P. Somogyi. 1999a. Alterations in the expression of $GABA_A$ receptor subunits in cerebellar granule cells after the disruption of the $\alpha 6$ subunit gene. *Eur. J. Neurosci.* 11:1685–1697.

Nusser, Z., S. G. Cull-Candy, and M. Farrant. 1997. Differences in synaptic $GABA_A$ receptor number underlie variation in GABA mini amplitude. *Neuron.* 19:697–709.

Nusser, Z., N. Hajos, P. Somogyi, and I. Mody. 1998. Increased number of synaptic $GABA_A$ receptors underlies potentiation at hippocampal inhibitory synapses. *Nature.* 395:172–177.

Nusser, Z., W. Sieghart, D. Benke, J.-M. Fritschy, and P. Somogyi. 1996. Differential synaptic localization of two major γ-aminobutyric acid type A receptor α subunits on hippocampal pyramidal cells. *Proc. Natl. Acad. Sci. U.S.A.* 93:11939–11944.

Nusser, Z., W. Sieghart, and I. Mody. 1999b. Differential regulation of synaptic $GABA_A$ receptors by cAMP-dependent protein kinase in mouse cerebellar and olfactory bulb neurones. *J. Physiol. (Lond.).* 521: 421–435.

Palay, S. L., and V. Chan-Palay. 1974. Cerebellar Cortex: Cytology and Organization. Springer Verlag, Berlin.

Perrais, D., and N. Ropert. 1999. Effect of zolpidem on miniature IPSCs and occupancy of postsynaptic GABAA receptors in central synapses. *J. Neurosci.* 19:578–588

Persohn, E., P. Malherbe, and J. G. Richards. 1992. Comparative molecular neuroanatomy of cloned $GABA_A$ receptor subunits in the rat CNS. *J. Comp. Neurol.* 326:193–216.

Redman, S. 1990. Quantal analysis of synaptic potentials in neurons of the central nervous system. *Physiol. Rev.* 70:165–198.

Sato, K., H. Kiyama, and M. Tohyama. 1993. The differential expression patterns of messenger RNAs encoding non-*N*-methyl-D-aspartate receptor subunits (GluR1–4) in the rat brain. *Neuroscience.* 52:515–539.

Schachter, S. C. 1999. Tiagabine. *Epilepsia.* 40:S17–S22.

Silver, R. A., S. G. Cull-Candy, and T. Takahashi. 1996. Non-NMDA glutamate receptor occupancy and open probability at a rat cerebellar synapse with single and multiple release sites. *J. Physiol. (Lond.).* 494:231–250.

Stevens, C. F. 1993. Quantal release of neurotransmitter and long-term potentiation. *Cell/Neuron.* Suppl 1:55–63.

Suzdak, P. D., K. Frederiksen, K. E. Andersen, P. O. Sorensen, L. J. Knutsen, and E. B. Nielsen. 1992. NNC-711, a novel potent and selective γ-aminobutyric acid uptake inhibitor: pharmacological characterization. *Eur. J. Pharmacol.* 224:189–198.

Traynelis, S. F., and F. Jaramillo. 1998. Getting the most out of noise in the central nervous system. *Trends Neurosci.* 21:137–145.

Traynelis, S. F., R. A. Silver, and S. G. Cull-Candy. 1993. Estimated conductance of glutamate receptor channels activated during EPSCs at the cerebellar mossy fiber-granule cell synapses. *Neuron.* 11:279–289.

Valtorta, F., R. Fesce, F. Grohovaz, C. Haimann, W. P. Hurlbut, N. Iezzi, F. Torri Tarelli, A. Villa, and B. Ceccarelli. 1990. Neurotransmitter release and synaptic vesicle recycling. *Neuroscience.* 35:477–489.

Wisden, W., D. J. Laurie, H. Monyer, and P. H. Seeburg. 1992. The distribution of 13 $GABA_A$ receptor subunit mRNAs in the rat brain. I. Telencephalon, diencephalon, mesencephalon. *J. Neurosci.* 12: 1040–1062.

Zador, A. 1998. Impact of synaptic unreliability on the information transmitted by spiking neurons. *J. Neurophysiol.* 79:1219–1229.